Magneto-optics enhancement with gain-assisted plasmonic subdiffraction chains

D. G. Baranov,[1,2] A. P. Vinogradov,[1,2,3] and A. A. Lisyansky[4,5,]*

[1]*Moscow Institute of Physics and Technology, 9 Institutskiy per., Dolgoprudniy 141700, Russia*
[2]*All-Russia Research Institute of Automatics, 22 Sushchevskaya, Moscow 127055, Russia*
[3]*Institute for Theoretical and Applied Electromagnetics, 13 Izhorskaya, Moscow 125412, Russia*
[4]*Department of Physics, Queens College of the City University of New York, Queens, New York 11367, USA*
[5]*The Graduate Center of the City University of New York, New York, New York 10016, USA*
*Corresponding author: alexander.lisyansky@qc.cuny.edu

We study enhancement of the magneto-optical (MO) effect in subdiffraction plasmonic chains. We show that, in a periodic chain of the plasmonic nanoparticles embedded in an MO medium, propagation of a guided mode is accompanied by rotation of electric dipoles (the Faraday effect). The angle of rotation per unit length is an order of magnitude greater than that in the same bulk MO medium. We also demonstrate that the effect of Joule losses can be significantly reduced by using a gain-assisted chain composed of active core-shell nanoparticles (spasers). The guided mode in such an array of MO spasers exhibits high values of the Faraday rotation and propagation length.   © 2015 Optical Society of America

OCIS codes: (230.3810) Magneto-optic systems; (250.5403) Plasmonics; (130.2790) Guided waves; (350.4238) Nanophotonics and photonic crystals.

http://dx.doi.org/10.1364/JOSAB.32.000281

1. INTRODUCTION

The magneto-optical (MO) effect is widely used to manipulate light. Time-reversal symmetry breaking due to the presence of a magnetic field in MO materials offers various opportunities for the effective polarization conversion and optical isolation [1]. However, the MO response of natural media is relatively weak so that enhancements of MO properties are highly desirable. Recently, a number of approaches to MO effect enhancing have been proposed (for a review see, e.g., [2]). One of these incorporates layered systems [3] for which a rigorous eigenmodes analysis can be performed. In these structures, at a certain frequency, multiple refraction of light from interfaces between magnetic and nonmagnetic layers may result in the Fabry–Perot resonance and the enhancement of the Faraday rotation. The enhancement is due to the fast growth of the phase, which changes by π when the frequency passes through the resonance. Thus, instead of a small bulk value of the Faraday angle, one can obtain the value of the order of $\pi/2$ [2,4].

MO effects can also be enhanced in metallic systems. The effect of the plasmon resonance of charge carries on the MO response was first analyzed in [5] in which the strong enhancement of the Kerr effect in bulk metal near the plasma frequency was reported (see also [6,7]). Strong coupling between traveling surface plasmons in metals and MO effects was also demonstrated by using the total internal reflection technique in [8].

In MO composites containing metal nanoparticles (NPs), localized surface plasmon excitation also promises to strongly enhance the MO response of these materials [9–14]. A different type of MO enhancement attributed to the phenomenon of extraordinary optical transmittance was observed in systems with magnetic metallic gratings [15,16] and perforated periodic structures [17–19].

In this paper, we propose another approach to the resonance MO enhancement. This approach incorporates properties of so-called subdiffraction chains (SDCs) [20]. We investigate the enhancement of the Faraday rotation in linear periodic SDCs of plasmonic NPs embedded in an MO host medium. We show that, in this system, the Faraday effect can be strongly enhanced and discuss how to compensate for Joule losses in metallic NPs.

Periodic linear chains of near-field coupled plasmonic NPs have been studied extensively since the original work of Quinten *et al.* [20]. It was shown that a 1D NP array supports guided modes due to near-field interactions between adjacent NPs. At first, only quasi-static interactions with the nearest neighbors were considered [21,22]. Then, effects of retardation that have a significant impact on the dispersion characteristics of long wavelength guided modes were taken into account [23]. Modes of finite 1D [24], infinite 2D [25], and 3D [26] as well as disordered arrays [27] of NPs were also investigated.

Intriguing properties of subdiffraction chains composed of magnetized plasmonic NPs have been studied recently. In particular, the combination of the MO activity and geometrical chirality of a chain, made of twisted ellipsoidal NPs, have been shown to lead to a one-way subdiffraction waveguide [28,29]. However, the Faraday effect has not been investigated in these systems. A detailed theoretical investigation of magnetic plasmonic NPs clusters has been presented in [30], in which the Faraday rotation and circular dichroism are studied for the configurations of dimers, helices, and random NP gas. In all these systems, the enhancement of the Faraday rotation

due to the plasmonic resonance is predicted. Similar structures consisting of Au/Ag NPs embedded into yttrium-iron garnet thin film were successfully fabricated in [31,32]. Although the structures presented in those works were random rather than periodic clusters of NPs, we expect that a periodic system also can be fabricated. For example, a linear chain of plasmonic particles can be deposited on a MO substrate via electron beam lithography [33]; after that, another layer of a MO material can be deposited on the whole MO substrate/particles structure [32].

The paper is organized as follows: In Section 2, we derive an analytical expression for the polarizability of an isotropic spherical NP embedded into a gyrotropic medium. In Section 3, we consider a 1D periodic array of silver NPs in a gyrotropic host medium. In Section 4, we analyze guided modes of a 1D gain-assisted MO SDC. The results are summarized in the Conclusion.

2. NANOPARTICLE EMBEDDED INTO A MAGNETO-OPTICAL MEDIUM

We study a periodic chain of spherical metallic (silver) NPs of radius R and interparticle separation L embedded into a MO host medium (Bi:YIG). This structure is shown schematically in Fig. 1. We assume that the chain is aligned in the direction of the MO medium magnetization vector, which is parallel to the z axis. Thus, the permittivity tensor of the host medium has the form

$$\hat{\varepsilon}_{\text{ext}} = \begin{pmatrix} \varepsilon & ig & 0 \\ -ig & \varepsilon & 0 \\ 0 & 0 & \varepsilon \end{pmatrix}. \qquad (1)$$

We model the subwavelength NPs as polarizable dipoles. This approximation is valid if (1) sizes of the NPs are much smaller than the light wavelength inside the NP material and (2) higher multipole resonances of NPs are not excited [23]. Both conditions are satisfied in our analysis. In order to find guided modes of the dipolar chain, one needs to know two essential characteristics: dipole polarizability of a spherical inclusion in a MO medium and the Green's function of an electric dipole in a MO medium that includes both far and near fields. Although dispersion of the guided modes of the SDC near the light cone is strongly affected by the far-field interaction [33], far from the light cone (for wavevectors $k \gg k_0$, where $k_0 = \text{Re}(n_{\text{Bi:YIG}}\omega/c)$ is the wavevector of a plane wave
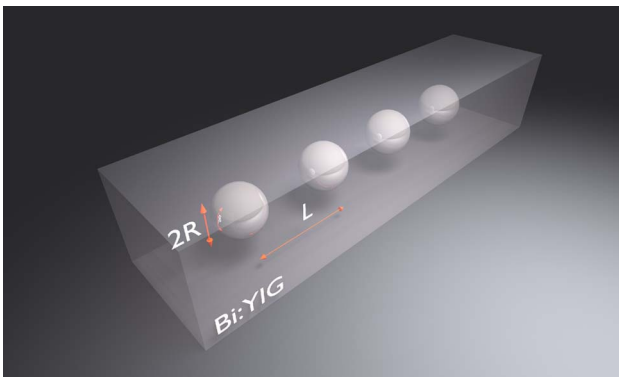

Fig. 1.   Geometry of the problem: a periodic array of silver nanospheres each of radius R with interparticle distance L embedded into an MO medium.

traveling in the host medium) the dispersion is well described by near-field interactions of nearest neighbors [23], which we use below. The dipole polarizability is calculated in the quasistatic approximation.

The electrostatic potential φ in the surrounding MO host obeys the equation

$$\text{div } \mathbf{D} = \nabla \cdot (\hat{\varepsilon}_{\text{ext}} \nabla \varphi) = 0. \qquad (2)$$

Nondiagonal terms in the permittivity tensor in Eq. (1), $ig\partial_{xy}\varphi$ and $-ig\partial_{yx}\varphi$, cancel out, and Eq. (2) transforms into the Laplace equation:

$$\varepsilon \Delta \varphi = 0. \qquad (3)$$

This allows us to conclude that the near field of a point electric dipole $\mathbf{d}$ in an MO medium is simply the near field of an electric dipole embedded in an isotropic host medium with permittivity ε:

$$\mathbf{E}_{\text{near}}(\mathbf{r}) = -\frac{\mathbf{d}}{\varepsilon r^3} + 3\frac{(\mathbf{d} \cdot \mathbf{n})\mathbf{n}}{\varepsilon r^3}. \qquad (4)$$

Now, let us find the polarizability dyadic of an isotropic sphere with permittivity ε_{int} embedded into a MO medium. The sphere is subjected to an external oscillating homogenous field $\mathbf{E}e^{-i\omega t}$. Below, we omit the harmonic time dependence of the electric field $e^{-i\omega t}$. The electrostatic potential outside the sphere can be represented as

$$\varphi_{\text{ext}} = -\mathbf{E}\mathbf{r} + (\hat{A}\mathbf{E})\mathbf{r}/r^3, \qquad (5)$$

where $\hat{A}$ is an unknown tensor, which relates the applied electric field $\mathbf{E}$ and the induced dipole moment of the sphere $\mathbf{d}$. The electric field in the surrounding medium is given by

$$\mathbf{E}_{\text{ext}} = -\nabla\varphi_{\text{ext}} = \mathbf{E} - \hat{A}\mathbf{E}/r^3 + 3(\hat{A}\mathbf{E} \cdot \mathbf{n})\mathbf{n}/r^3, \qquad (6)$$

where $\mathbf{E}_{\text{ext}} \times \mathbf{n} = \mathbf{E} \times \mathbf{n} - \hat{A}\mathbf{E} \times \mathbf{n}/r^3$. The normal component of the displacement $\mathbf{D}$, which is needed in the following calculations, can be expressed through the incident field $\mathbf{E}$ as

$$\mathbf{D}_{\text{ext}} \cdot \mathbf{n} = \hat{\varepsilon}_{\text{ext}}\mathbf{E}_{\text{ext}} \cdot \mathbf{n}$$
$$= \varepsilon(\mathbf{E} \cdot \mathbf{n} + 2\hat{A}\mathbf{E} \cdot \mathbf{n}/r^3) + \hat{G}(\mathbf{E} \cdot \mathbf{n} - \hat{A}\mathbf{E} \cdot \mathbf{n}/r^3), \qquad (7)$$

with $\hat{G}$ being the nondiagonal part of the permittivity tensor $\hat{\varepsilon}$. The electric field inside the spherical inclusion can be written in the form

$$\mathbf{E}_{\text{int}} = \hat{B}\mathbf{E}, \qquad (8)$$

where $\hat{B}$ is an as yet undetermined tensor. Using electromagnetic boundary conditions for Maxwell's equations, we obtain the system of equations

$$\hat{I} - \hat{A}/R^3 = \hat{B},$$
$$\varepsilon(\hat{I} + 2\hat{A}/R^3) + \hat{G}(\hat{I} - \hat{A}/R^3) = \varepsilon_{\text{int}}\hat{B}, \qquad (9)$$

which allows us to determine the tensor $\hat{A}$:

$$\hat{A} = R^3(\varepsilon_{\text{int}}\hat{I} - \hat{\varepsilon}_{\text{ext}})(\varepsilon_{\text{int}}\hat{I} + 2\hat{\varepsilon}_{\text{ext}} - 3\hat{G})^{-1}. \quad (10)$$

The dipole polarizability relates the incident field and the induced dipole moment of an NP as $\mathbf{d} = \hat{\alpha}\mathbf{E}$. Comparing Eqs. (4) and (6), we conclude that $\hat{\alpha} = \varepsilon\hat{A}$. Notably, the form of Eq. (10) differs significantly from the expression for the quasi-static polarizability of an MO particle inside an isotropic medium, which takes the form of the Clausius–Mossotti relation [34]. Unlike the latter, here the antidiagonal term $3\hat{G}$ singles out in the denominator, so that the whole expression cannot be written in the Clausius–Mossotti form. The elements of the dipole polarizability dyadic are given by

$$\alpha_{xx} = \alpha_{yy} = \varepsilon R^3 \frac{\varepsilon_{\text{int}}^2 + \varepsilon_{\text{int}}\varepsilon - 2\varepsilon^2 - g^2}{\varepsilon_{\text{int}}^2 + 4\varepsilon_{\text{int}}\varepsilon + 4\varepsilon^2 - g^2},$$

$$\alpha_{xy} = -\alpha_{yx} = \varepsilon R^3 \frac{3i\varepsilon g}{\varepsilon_{\text{int}}^2 + 4\varepsilon_{\text{int}}\varepsilon + 4\varepsilon^2 - g^2},$$

$$\alpha_{zz} = \varepsilon R^3 \frac{\varepsilon_{\text{int}} - \varepsilon}{\varepsilon_{\text{int}} + 2\varepsilon}. \quad (11)$$

and the polarizability dyadic is represented as

$$\hat{\alpha} = \begin{pmatrix} \alpha_{xx} & \alpha_{xy} & 0 \\ -\alpha_{xy} & \alpha_{xx} & 0 \\ 0 & 0 & \alpha_{zz} \end{pmatrix}. \quad (12)$$

In the subspace $E_z = 0$, we find two eigenvalues of the polarizability tensor $\hat{\alpha}$:

$$\alpha_+ = \alpha_{xx} + i\alpha_{xy} = \varepsilon R^3 \frac{\varepsilon^{\text{int}} - \varepsilon + g}{2\varepsilon + \varepsilon^{\text{int}} + g},$$

$$\alpha_- = \alpha_{xx} - i\alpha_{xy} = \varepsilon R^3 \frac{\varepsilon^{\text{int}} - \varepsilon - g}{2\varepsilon + \varepsilon^{\text{int}} - g}, \quad (13)$$

so that $\hat{\alpha}\mathbf{E}_+ = \alpha_+\mathbf{E}_+$ and $\hat{\alpha}\mathbf{E}_- = \alpha_-\mathbf{E}_-$, where $\mathbf{E}_+ = (1, i, 0)^T$ and $\mathbf{E}_- = (1, -i, 0)^T$ are the two eigenvectors of the polarizability tensor with $E_z = 0$. These two eigenvectors correspond to circularly polarized incident light. The third eigenvalue is equal to α_{zz} and is of no interest here because it corresponds to the electric field polarized along the magnetization vector for which no Faraday rotation can be observed.

3. GUIDED MODES OF A MAGNETO-OPTICAL SUBDIFFRACTION CHAIN

Having calculated all the quantities in Section 2, one may find guided modes of an MO SDC. We seek guided solutions in the form $\mathbf{d}_n \sim e^{ikz_n}$. As shown earlier [21], SDCs can support guided modes with both transverse (T) or longitudinal (L) polarizations. Since we are interested in the Faraday rotation, which is naturally observed for the T-polarization, we limit ourselves to analyzing this particular polarization. Polarizations of the electric field and the NP dipole moment for the T-polarization are $\mathbf{E} = (E_x, E_y, 0)$ and $\mathbf{d} = (d_x, d_y, 0)$, respectively. For the transverse polarization of the electric field $(\mathbf{d} \cdot \mathbf{r}_n) = 0$, where $\mathbf{r}_n$ points along the chain, so that only a single term remains in Eq. (4).

Consistent analysis of the problem requires calculation of the total local electric field acting on an NP. This field is the sum of fields due to *all other dipoles in the chain*. However, as noted above, in the region far from the light cone, where $k \gg k_0$, the tight-binding approximation gives reasonable

results, which may be utilized to further analyze the problem. In the tight-binding approximation, the electric field applied to the nth point dipole is the sum of the fields created by the two neighboring particles:

$$\mathbf{E}_n = -\frac{\mathbf{d}_{n-1} + \mathbf{d}_{n+1}}{\varepsilon L^3} = -\frac{e^{-ikL}\hat{\alpha}\mathbf{E}_n + e^{ikL}\hat{\alpha}\mathbf{E}_n}{\varepsilon L^3}. \quad (14)$$

Equation (14) represents an eigenvalue problem for the polarizability tensor (12) of a metallic inclusion. Substituting the eigenvalues in Eq. (13) into Eq. (14) for the two different eigenvectors $\mathbf{E}_+$ and $\mathbf{E}_-$, we obtain a pair of dispersion relations:

$$\mathbf{E}_\pm = -\frac{e^{-ikL} + e^{ikL}}{\varepsilon L^3}\alpha_\pm\mathbf{E}_\pm = -\frac{2\cos kL}{\varepsilon L^3}\alpha_\pm\mathbf{E}_\pm. \quad (15)$$

Equation (15) leads to explicit expressions for the guided mode wavevectors:

$$k_\pm = \frac{1}{L}\cos^{-1}\left(\frac{-\varepsilon L^3}{2\alpha_\pm}\right). \quad (16)$$

According to Eq. (16), two guided modes, which we refer to as "+" and "−," have circular polarizations of the electric field. Taking into account different values of the Bloch wavevectors and circular polarization of the electric field, one may anticipate that propagation of an excitation along the chain is accompanied by the Faraday rotation.

First, we present the dispersion curves for the idealized case of lossless silver NPs embedded into a lossless MO medium for $R = 10$ nm and $L = 4R$. Although lossless materials, especially plasmonic metals, are not available, this consideration allows us to estimate how sensitive Faraday rotation enhancement is to Joule loss. The two dispersion curves of guided modes of a 1D chain of silver NPs are shown in Fig. 2. Experimental data from [35] and [36] were adopted to approximate permittivity of silver and Bi:YIG, respectively. One can see that, in a relatively narrow frequency region between 2.25 and 2.35 eV, the plasmon resonance gives rise to the propagation band of an array of NPs. The two dispersion curves are split due to MO activity of the host medium, which manifests itself in different polarizabilities α_+ and α_-.

Note that the dispersion curves obtained from Eqs. (16) represent *backward waves* so that their the group velocity and
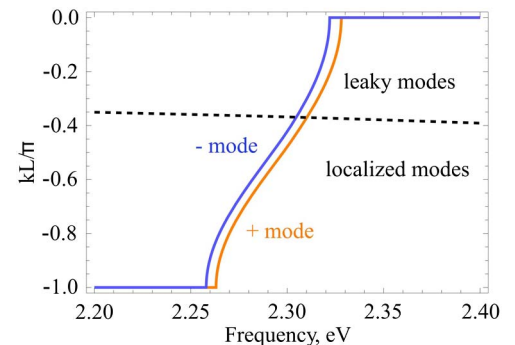

Fig. 2. Dispersion curves of the 1D chain of lossless silver NPs embedded into Bi:YIG. The dashed line indicates the light cone with $|k| = \text{Re } n_{\text{Bi:YIG}}\omega/c$, which separates the regions of localized and leaky modes.

the wavevector have opposite signs. In all figures, we plot the frequency dispersion of MO chain guided modes in such a way that the group velocity is always positive, whereas the real part of wavevector is negative.

As mentioned above, we search for guided solutions only in the region for which $|k| > k_0$. Such excitations (bound modes) can propagate along the chain without radiative losses, while leaky modes with $|k| < k_0$ experience strong radiative decay. When Joule losses are present in the system, all modes couple to free space radiation. This happens because the wavevector of an eigenmode is always complex-valued in the lossy case, so that there is always energy flow in direction normal to the chain. Nevertheless, modes with $|\text{Re}(k)| > k_0$ experience much slower radiative decay due to their localized nature, as indicated in [37]. For that reason, in what follows we refer to such solutions as localized modes.

In certain cases, the quasi-static approximation is not very accurate for description of multiple scattering effects, even for subwavelength scatterers [33,38]. To validate our assumption, we compare the results of the quasi-static calculation with the results of the exact calculation, which takes into account the effect of retardation (i.e., an incident field is created by all NPs in the chain). The results are calculated for the case of a lossless nonmagnetic host medium with isotropic permittivity given by the diagonal element of tensor (1). Figure 3 shows the quasi-static solution given by Eq. (16) for nonmagnetic media and the exact retarded solution, adopted from [23]. Although in [23] the dispersion equation was obtained for 50 nm NPs, it equally applies to our case of 10 nm radius particles, since the point dipole approximation is even more accurate for smaller particles. The results indicate that in the operation region far from the light line, the quasi-static and full-retarded solutions show a reasonable agreement. Although guided modes of a SDC within the operation region have a lower group velocity than is predicted by

the quasi-static approximation, it should not dramatically affect the Faraday rotation.

The Faraday rotation of the polarization by an MO chain per unit length can be estimated as $\theta = (k_+ - k_-)/2$. Indeed, when a chain is excited at its input by a linearly polarized electric field $E_{\text{input}} = (1, 0, 0)^T$, which is the most common situation, this polarization is decomposed into two eigenmodes of a chain with equal amplitudes:

$$E_{\text{input}} = \frac{1}{2}[(1, i, 0)^T e^{ik_+ z} + (1, -i, 0)^T e^{ik_- z}]|_{z=0}. \quad (17)$$

This is similar to the case of a uniform MO medium, for which the polarization rotation is also given by the above expression. To obtain an estimate for θ, we the calculate Faraday rotation per length of the 10-nanoparticle chain, which is given by $\theta = 10L \cdot (k_+ - k_-)/2$. This estimation is plotted in Fig. 5.

As we can see from Fig. 4, the Faraday rotation is dramatically increased compared to bulk Bi:YIG. Notably, the Faraday rotation increases even more in the vicinity of the bandgap. This behavior can be understood from Fig. 2. Indeed, near the band edge of one mode, while the other is still propagating, the group velocity, $v_g = \partial\omega/\partial k$, of this mode rapidly drops to zero, which results in a larger distance (and a larger wavevector difference) between the two modes. As a consequence, the Faraday rotation angle θ increases as well.

The remarkable property of dispersion law (16) is its *scaling behavior*. One may fix the ratio R/L and tend both NP's radius, R, and interparticle distance, L, to zero. Then, wavevectors of "+" and "−" guided modes proportionally increase as $1/L$. The Faraday rotation angle, θ, increases as well. In fact, the factor, which limits such a scaling behavior, is the applicability of the concept of permeability. When an NP is small enough (<5 nm), the description of the NP in terms of permittivity tensor (1) is not applicable, and its electromagnetic response can no longer be described by the polarizability $\hat{\alpha}$ (13). (We are appreciative to Antonio García-Martín who has directed our attention to this fact.)

Dispersions of guided modes and the Faraday rotation in the realistic case of lossy NPs and the host medium are
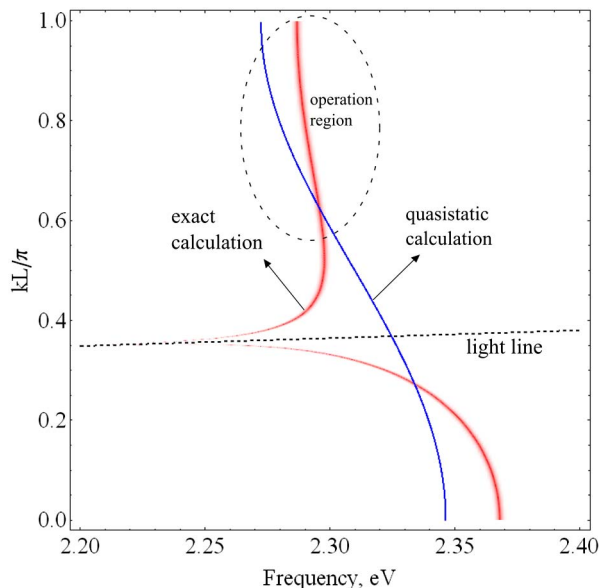

Fig. 3.   Results of the quasi-static calculation (blue solid line) compared with the exact full retarded solution (red solid line) for a nonmagnetic lossless host medium adopted from [23] adjusted for NPs size used in our calculations. Within the operation region of the MO chain, both solutions show reasonable agreement.
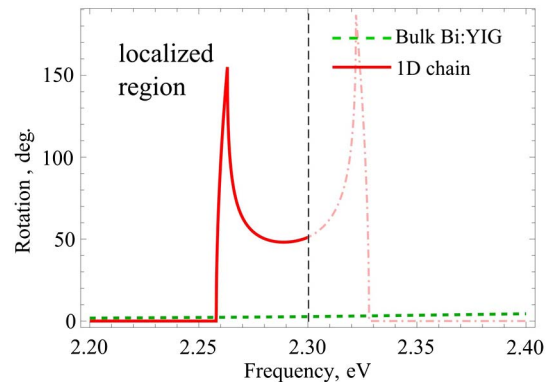

Fig. 4.   Estimation for the Faraday rotation in a 1D chain of length $10L$ of lossless silver NPs (red solid curve) and for bulk Bi:YIG (green dashed curve). The vertical dashed line separates the localized and leaky regions of an MO chain. In the leaky region, the Faraday rotation in an MO chain is shown by a dotted–dashed curve. The Faraday rotation provided by the bulk MO medium is less than 5 deg in the whole frequency range.
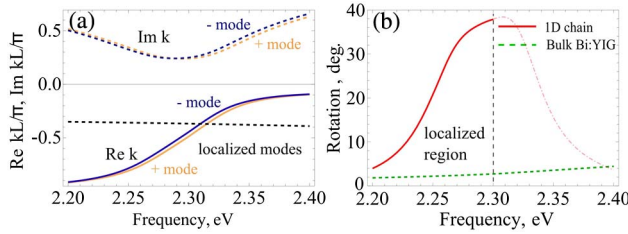
Fig. 5. (a) Dispersion of guided modes of lossy MO chain. Real and imaginary parts of the Bloch wavevectors $k_\pm$ are shown by solid and dashed curves, respectively. Black dashed line is the light line; modes below this line are localized modes. (b) Estimates for the Faraday rotation angles per length $10L$ for a lossy MO chain (solid curve) and for bulk Bi:YIG (dashed curve).

presented in Fig. 5. Overall, Joule losses drastically quench the effect. The propagation band becomes less pronounced. The propagation length of the guided mode can be estimated as $l_{prop} = |Im\,k|^{-1}$. As seen from Fig. 5(a), the propagation distance is of the order of the interparticle distance L. Thus, the wave is absorbed before it reaches the end of the chain. Joule losses also have strong impact on the Faraday rotation angle: the maximum value of the Faraday rotation in a chain of lossy particles is several times lower than that of lossless particles.

The results presented in this section allow us to conclude that, for the enhancement of the Faraday rotation, it is critical to have low value of Joule losses. A practical way of achieving this is compensation of the effect of losses. In the next section, we show how Joule loss can be minimized in gain-assisted chains formed by composite core-shell NPs.

4. GAIN-ASSISTED SUBDIFFRACTION MAGNETO-OPTICAL CHAIN

The problem of compensation for strong attenuation in SDCs due to Joule damping has been addressed in the literature [39–41]. In [39], amplification is provided by gain in the host medium, into which the plasmonic chain is embedded, while, in [41], the authors consider a chain formed by composite core-shell NPs in which gain is provided by active cores. In [40], both approaches are analyzed and compared. We follow the second approach and consider an SDC made of composite gain-assisted NPs. A single composite NP is schematically depicted in Fig. 6. It consists of the silver spherical core of radius r_1 and the gain shell of radius r_2. The layout of a chain is the same as in the previous section: NPs are embedded into
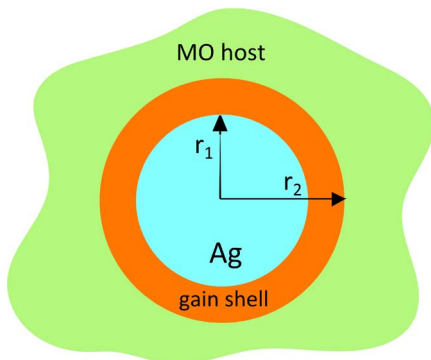

Fig. 6. Schematic of a gain-assisted core-shell NP constituting a gain-assisted MO chain.

Bi:YIG with the interparticle distance L and with the magnetization vector of the MO medium parallel to the chain axis.

Combination of a gain medium and a MO plasmonic resonator leads to the formation of the MO spaser [42] (for a review of spasers, see [43]). Above the threshold, it has two lasing modes with circular polarizations of dipole moments and different lasing frequencies. Here, we are concerned with the below-threshold regime of the MO spaser, when gain is insufficient to support spasing.

The electromagnetic response of the gain medium below the lasing threshold can be described with an effective permittivity, which is deduced from the Maxwell–Bloch equations [44–46]:

$$\varepsilon_{gain}(\omega) = \varepsilon_0 + D_0 \frac{\omega_0}{\omega} \frac{1}{i + \frac{\omega^2 - \omega_0^2}{2\omega\Gamma}}. \qquad (18)$$

In the above formula, Γ is the emission linewidth of the gain medium, ω_0 is the emission frequency, and $D_0 = 4\pi|\mu|^2 n/(\hbar\Gamma)$ is a dimensionless characteristic of the pump rate, which is proportional to the volume population inversion of the quantum emitters n and squared transition dipole moment of a quantum emitter $|\mu|^2$. The gain medium can be realized either as a collection of dye molecules or quantum dots. However, as we show below, gain provided by typical organic dye, even at full inversion of chromophores, is not sufficient for loss compensation. For this reason, quantum dots have to be used in order to provide gain. In calculations, the value of the emission linewidth Γ is set to $\Gamma = 20$ meV [47], background permittivity of the gain medium is set to $\varepsilon_0 = 4$, and its emission frequency is tuned to the narrow propagation band of SDC. The radii of the core-shell NP used in the following calculations are $r_2 = 10$ nm and $r_1 = 0.8r_2$, respectively. For the parameters specified above, the propagation band of the SDC arises in the frequency region between 2.4 and 2.5 eV; for that reason, the emission frequency is set to $\omega_0 = 2.45$ eV.

Following the same procedure as in Section 3, we find the dispersion law of guided modes in the tight-binding approximation:

$$k_\pm = \frac{1}{L} \cos^{-1}\left(\frac{-\varepsilon L^3}{2\alpha_\pm^{core-shell}}\right), \qquad (19)$$

where $\alpha_\pm^{core-shell}$ are eigenvalues of the dipole polarizability tensor of the composite core-shell NP placed in the MO medium. This tensor is found in the same fashion as for the case of a simple spherical NP in a MO medium. Expressions for these two eigenvalues can be found in Appendix A.

Basically, in most applications, a nonzero output signal and dipole moments of NPs are only generated by a nonzero input signal. At the same time, in gain systems, when the pump rate exceeds the threshold, an electrodynamic system of dipole scatterers may have lasing states, at which the system possesses nonzero dipole moments without any incident radiation. Such a regime of operation is inappropriate for the purpose of the polarization control. Below, we assume that the pump rate D_0 is smaller than the specific lasing threshold.

The threshold of a single NP appears as a pole of dipole polarizability, namely, as a pole of one of its eigenvalues. Since dyadic $\hat{\alpha}^{core-shell}$ has three different eigenvalues corresponding to different polarizations of incident light, each

eigenvalue has its own threshold and corresponds to the unique configuration of the lasing mode. To prevent lasing, one should choose the pump rate D_0 below the lowest threshold $D_{\min}$.

The situation changes for a system of interacting NPs with gain. In such a system, due to the effect of multiple scattering, thresholds for each mode change. In this paper, we do not establish a general condition for lasing in a system of interacting dipoles [48]. Instead, we use a less general but more strict condition, which guarantees that no lasing occurs in a periodic chain.

The scattering behavior of a composite NP is described by dipole polarizability $\hat{\alpha}^{\text{core-shell}}$. This dyadic may be diagonalized so that scattering may be described by its three elements in the diagonal basis: $\alpha_+^{\text{core-shell}}$, $\alpha_-^{\text{core-shell}}$ and $\alpha_{zz}^{\text{core-shell}}$. When imaginary parts of these quantities are all positive,

$$\text{Im}\,\alpha_+^{\text{core-shell}} > 0, \quad \text{Im}\,\alpha_-^{\text{core-shell}} > 0, \quad \text{Im}\,\alpha_{zz}^{\text{core-shell}} > 0, \quad (20)$$

scattering of incident light for any possible polarization is accompanied by dissipation, since the dissipated power is given by

$$W = \frac{\omega}{2}(\text{Im}\,\alpha_+^{\text{core-shell}}|E_+|^2 + \text{Im}\,\alpha_-^{\text{core-shell}}|E_-|^2 + \text{Im}\,\alpha_{zz}^{\text{core-shell}}|E_z|^2). \quad (21)$$

On the other hand, for a system of dissipative dipole scatterers, a lasing mode cannot arise regardless of the value of gain in each NP. Indeed, under this condition, the total dissipated power in the system is always positive, and a lasing mode cannot exist.

Relying on this simple argument, we limit the range of the pump rate to the values for which inequalities (20) hold. The maximum value of the pump rate, at which these three conditions are satisfied, we denote by D_{diss}. For values of the pump rate such that $D_0 < D_{\text{diss}}$, the core-shell NP is strictly dissipative. Although we cannot analytically establish the value of D_{diss} due to the very complex form of the expression for $\hat{\alpha}^{\text{core-shell}}$, numerical calculations for parameters of the NP introduced above indicate that $0.3 < D_{\text{diss}}$. From Fig. 7, one can see that for $D_0 = 0.3$, all three eigenvalues demonstrate dissipative behavior. For any $D_0 < 0.3 < D_{\text{diss}}$, all three eigenvalues have positive imaginary parts.

In Fig. 8, we plot dispersion of guided modes of the gain-assisted MO chain for zero pump rate, Figs. 8(a) and 8(b),
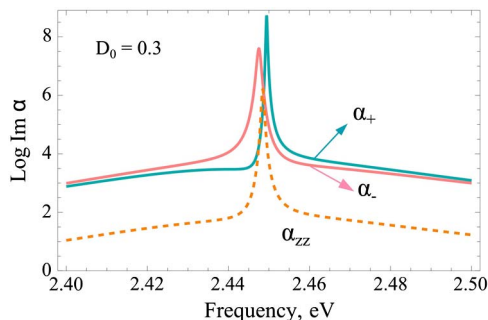
Fig. 7. Eigenvalues of polarizability dyad $\hat{\alpha}^{\text{core-shell}}$ for the pump rate $D_0 = 0.3$. Since imaginary parts of all three eigenvalues are positive, the system is dissipative and does not lase.
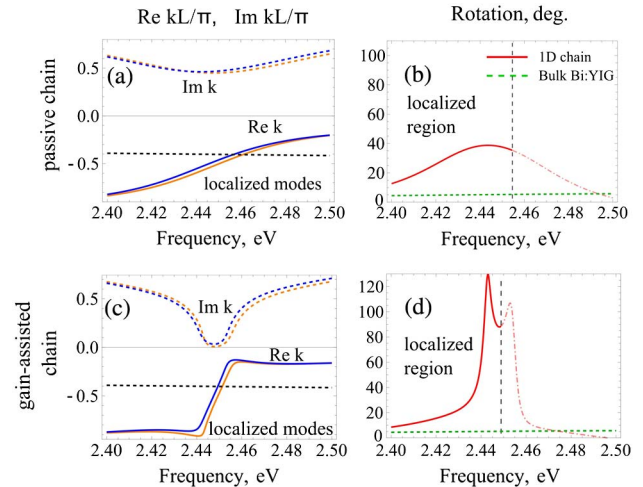
Fig. 8. Left panel: dispersion of guided modes of composite core-shell NPs embedded into YIG. Black dashed line is the light cone. Right panel: the Faraday rotation along the chain of length $10L$. Top: passive SDC with zero pump rate. Bottom: gain-assisted SDC with pump rate $D_0 = 0.3$.

and for the optimal value of the pump rate $D_0 = 0.3 < D_{\text{diss}}$, Figs. 8(c) and 8(d). The interparticle distance is $L = 4r_2$. Overall, patterns of dispersion curves and the Faraday rotation in a passive configuration with zero pump rate follow that of a passive chain of silver NPs [see Figs. 5(a) and 5(b)]. Real and imaginary parts of the wavevector have similar values; thus, the propagation distance of the guided mode is of the order of Bloch wavelength $2\pi/\text{Re}\,k$.

As the pump rate increases, the propagation band of an MO chain becomes narrower and more pronounced [Fig. 8(c)]. Note that, due to the gain layer at the surface of the silver NP, the plasmon resonance frequency slightly detunes from that of a bare silver NP immersed into a MO medium. This results in a different frequency region of the propagation band. At the same time, the Faraday rotation also increases with the rise of the pump rate D_0. For $D_0 = 0.3$, the Faraday rotation is comparable or greater than that in a lossless SDC [Fig. 8(d)].

Introducing gain allows one to increase the propagation distance of the guided modes [see Fig. 8(c)]. Due to our concerns on lasing mentioned above, we consider the case when both $\text{Im}\,\alpha_+$ and $\text{Im}\,\alpha_-$ are strictly positive. Therefore, the propagation length $l_{\text{prop}} = 1/\text{Im}\,k_{\pm}$ is always finite. The minimal value of the imaginary part of the wavevector, which we observe in the narrow propagation band of the gain-assisted SDC, corresponds to $\text{Im}\,k_{+,-}L/\pi < 0.03$. Let us estimate the fraction of the energy that reaches the end of chain of length $l = 10L$. Neglecting reflections from both ends of the 10-particle chain, the electric field intensity $I \sim E^2$ at the output of the chain can be estimated as $I_{\text{out}} = I_{\text{in}}\exp(-2\,\text{Im}\,k \cdot 10L) \approx 0.2I_{\text{in}}$. Thus, for the configuration considered here, approximately 20% of light would propagate along the chain to experience the Faraday rotation of approximately 90 deg, which is sufficient for applications in optical isolator schemes.

The pump rate of $D_0 = 0.3$ corresponds to the bulk gain coefficient $k'' = \text{Im}\sqrt{\varepsilon_{\text{gain}}}\omega_0/c \approx 10^4$ cm^{-1} at the resonance frequency. This level of gain is unattainable for organic dye, for which the maximum value of gain is of the order of 1.5×10^3 cm^{-1} [49]. However, for commercially available CdSe quantum dots, such value of the gain coefficient is easily
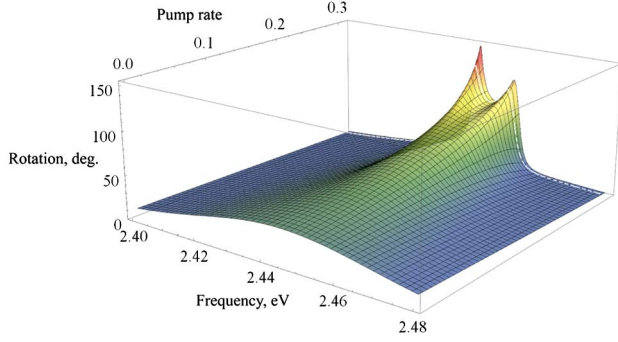
Fig. 9. Faraday rotation provided by a 10-particle chain as a function of frequency and the pump rate, D_0. The white dashed line indicates frequency-dependent rotation for $D_0 = 0.3$ used in Fig. 8(d).

achievable (see, e.g., [50]). Note that, due to quenching (non-radiative spontaneous decay of quantum emitters placed in close proximity to the plasmonic sphere), the resulting density of the population inversion n is smaller than for the case of an active medium in free space. As a result, polarizabilities of the composite particles as well as the dispersion curves may change. We simulated the effect of quenching by placing an additional layer of passive material with a dielectric constant ε_0 between the metal and the gain medium of thickness $t = 3$ nm. Calculations show that higher levels of the population inversion and gain D_0 are required for loss compensation; nevertheless, it is still attainable with CdSe quantum dots.

Figure 9 shows the Faraday rotation as a function of the frequency and the pump rate D_0. As the pump rate increases, the rotation angle also gradually increases within the propagation band. When the pump rate reaches the value close to $D_0 = 0.3$, the fine structure with two distinct peaks becomes visible. These peaks, as argued previously, correspond to the propagation band edge, at which the group velocity of one of the modes drops to zero.

5. CONCLUSION

We have carried out a theoretical study of the enhancement of the Faraday rotation in a 1D periodic chain of plasmonic NPs embedded into an MO medium. Using parameters for silver NPs and Bi-substituted yttrium iron garnet MO, we show that in this system, the angle of rotation of the direction of the NP dipole polarization increases by an order of magnitude compared to a bulk MO medium. Joule losses, however, substantially suppress this effect. We propose a way of compensating for these losses by covering NPs with gain layers, so that each NP turns into an MO spaser. The pump rate should be smaller than the spasing threshold. When the pumping frequency is tuned to the surface plasmon resonance, the imaginary part of the wavevector of the guided mode decreases, and the Faraday rotation is resonantly enhanced by an order of magnitude.

APPENDIX A: POLARIZABILITY OF A CORE-SHELL NANOPARTICLE IN A MAGNETO-OPTICAL MEDIUM

Consider a core-shell NP in an MO medium with inner and outer radii r_1 and r_2, respectively. To find polarizability dyadic of a composite core-shell NP embedded into an MO host in the quasi-static approximation, we write the electric field in the outer region (the MO host medium) as

$$\mathbf{E}_{\text{ext}}(\mathbf{r}) = \mathbf{E} - \frac{\hat{A}\mathbf{E}}{r^3} + 3\frac{(\hat{A}\mathbf{E} \cdot \mathbf{n})}{r^3}\mathbf{n}. \tag{A1}$$

The electric field in the shell can be represented as a sum of a homogenous field and point dipole-like contribution:

$$\mathbf{E}_{\text{shell}}(\mathbf{r}) = \hat{B}\mathbf{E} - \frac{\hat{C}\mathbf{E}}{r^3} + 3\frac{(\hat{C}\mathbf{E} \cdot \mathbf{n})}{r^3}\mathbf{n}. \tag{A2}$$

In Eqs. (A1) and (A2), tensors $\hat{A}$, $\hat{B}$, and $\hat{C}$ are unknown. The electric field in the core is represented only by the homogenous term, related to the incident field by another unknown tensor:

$$\mathbf{E}_{\text{core}}(\mathbf{r}) = \hat{F}\mathbf{E}. \tag{A3}$$

In the outer region, the near field of the NP has the same structure as that of a solid metallic NP in an MO medium [see Eq. (6)]; therefore, dyadic polarizability is expressed as $\hat{\alpha}^{\text{core-shell}} = \varepsilon\hat{A}$, and our goal is to find this tensor from the Maxwell's boundary conditions.

Again, normal and tangential components of the electric field and displacement, respectively, in the outer, shell, and core regions are expressed as

$$\mathbf{E}_{\text{ext}} \times \mathbf{n} = \mathbf{E} \times \mathbf{n} - \hat{A}\mathbf{E} \times \mathbf{n}/r^3,$$
$$\mathbf{D}_{\text{ext}} \cdot \mathbf{n} = \varepsilon(\mathbf{E} \cdot \mathbf{n} + 2\hat{A}\mathbf{E} \cdot \mathbf{n}/r^3) + \hat{G}(\mathbf{E} \cdot \mathbf{n} - \hat{A}\mathbf{E} \cdot \mathbf{n}/r^3),$$
$$\mathbf{E}_{\text{shell}} \times \mathbf{n} = \hat{B}\mathbf{E} \times \mathbf{n} - \hat{C}\mathbf{E} \times \mathbf{n}/r^3,$$
$$\mathbf{D}_{\text{shell}} \cdot \mathbf{n} = \varepsilon_{\text{gain}}(\hat{B}\mathbf{E} \cdot \mathbf{n} + 2\hat{C}\mathbf{E} \cdot \mathbf{n}/r^3),$$
$$\mathbf{E}_{\text{core}} \times \mathbf{n} = \hat{F}\mathbf{E} \times \mathbf{n},$$
$$\mathbf{D}_{\text{core}} \cdot \mathbf{n} = \varepsilon_{\text{core}}\hat{F}\mathbf{E} \cdot \mathbf{n}. \tag{A4}$$

Substituting these expressions into the boundary conditions, we arrive at the system of equations determining all introduced tensors:

$$\hat{I} - \hat{A}/r_2^3 = \hat{B} - \hat{C}/r_2^3,$$
$$\varepsilon(\hat{I} + 2\hat{A}/r_2^3) + \hat{G}(\hat{I} - \hat{A}/r_2^3) = \varepsilon_{\text{shell}}(\hat{B} + 2\hat{C}/r_2^3),$$
$$\hat{B} - \hat{C}/r_1^3 = \hat{F},$$
$$\varepsilon_{\text{shell}}(\hat{B} + 2\hat{C}/r_1^3) = \varepsilon_{\text{core}}\hat{F}. \tag{A5}$$

Finally, from this system we find tensor $\hat{A}$ and dipole polarizability $\hat{\alpha}^{\text{core-shell}}$. Explicit expressions for polarizability eigenvalues are

$$\alpha_{+}^{\text{core-shell}} = r_2^3\varepsilon\left(1 + \frac{3\varepsilon(\varepsilon_{\text{core}}(r_1^3 - r_2^3) + \varepsilon_{\text{shell}}(r_1^3 + 2r_2^3))}{\varepsilon_{\text{core}}((2\varepsilon + g)(r_1^3 - r_2^3) - \varepsilon_{\text{shell}}(2r_1^3 + r_2^3)) + \varepsilon_{\text{shell}}(-(2\varepsilon + g)(r_1^3 + 2r_2^3) + 2\varepsilon_{\text{shell}}(r_1^3 - r_2^3))}\right),$$

$$\alpha_{-}^{\text{core-shell}} = r_2^3\varepsilon\left(1 + \frac{3\varepsilon(\varepsilon_{\text{core}}(r_1^3 - r_2^3) + \varepsilon_{\text{shell}}(r_1^3 + 2r_2^3))}{\varepsilon_{\text{core}}((2\varepsilon - g)(r_1^3 - r_2^3) - \varepsilon_{\text{shell}}(2r_1^3 + r_2^3)) + \varepsilon_{\text{shell}}(-(2\varepsilon - g)(r_1^3 + 2r_2^3) + 2\varepsilon_{\text{shell}}(r_1^3 - r_2^3))}\right),$$

$$\alpha_{zz}^{\text{core-shell}} = r_2^3\varepsilon\left(1 - \frac{3\varepsilon(\varepsilon_{\text{core}}(r_1^3 - r_2^3) + \varepsilon_{\text{shell}}(r_1^3 + 2r_2^3))}{2\varepsilon_{\text{shell}}(\varepsilon(r_1^3 + 2r_2^3) + \varepsilon_{\text{shell}}(-r_1^3 + r_2^3)) + \varepsilon_{\text{core}}(2\varepsilon(-r_1^3 + 2r_2^3) + \varepsilon_{\text{shell}}(2r_1^3 + r_2^3))}\right), \tag{A6}$$

where $\alpha_{\pm}^{\text{core-shell}}$ correspond to polarizations of incident light $\mathbf{E} = (1, \pm i, 0)^T$ and $\alpha_{zz}^{\text{core-shell}}$ corresponds to incident light polarized along the magnetization vector of the MO host medium.

ACKNOWLEDGMENTS

REFERENCES

1. A. K. Zvezdin and V. A. Kotov, *Modern Magnetooptics and Magnetooptical Material* (Taylor & Francis, 1997).
2. A. P. Vinogradov, A. V. Dorofeenko, A. M. Merzlikin, Y. M. Strelniker, A. A. Lisyansky, A. B. Granovsky, and D. J. Bergman, "Enhancement of the Faraday effect in magnetophotonic crystals," in *Magnetophotonics From Theory to Applications*, M. Inoue, A. V. Baryshev, and M. Levy, eds. (Springer, 2013).
3. M. Inoue, K. Arai, T. Fujii, and M. Abe, "Magneto-optical properties of one-dimensional photonic crystals composed of magnetic and dielectric layers," J. Appl. Phys. **83**, 6768–6770 (1998).
4. M. J. Steel, M. Levy, and R. M. Osgood, "Photonic band gaps with defects and the enhancement of Faraday rotation," J. Lightwave Tech. **18**, 1297–1308 (2000).
5. H. Feil and C. Haas, "Magneto-optical Kerr effect, enhanced by the plasma resonance of charge carriers," Phys. Rev. Lett. **58**, 65–68 (1987).
6. Z. Q. Qiu, J. Pearson, and S. D. Bader, "Magneto-optic Kerr ellipticity of epitaxial Co/Cu overlayers and superlattices," Phys. Rev. B **46**, 8195–8200 (1992).
7. T. Katayama, Y. Suzuki, H. Awano, Y. Nishihara, and N. Koshizuka, "Enhancement of the magneto-optical Kerr rotation in Fe/Cu bilayered films," Phys. Rev. Lett. **60**, 1426–1429 (1988).
8. V. I. Safarov, V. A. Kosobukin, C. Hermann, G. Lampel, J. Peretti, and C. Marlière, "Magneto-optical effects enhanced by surface plasmons in metallic multilayer films," Phys. Rev. Lett. **73**, 3584–3587 (1994).
9. M. Abe and T. Suwa, "Surface plasma resonance and magneto-optical enhancement in composites containing multicore-shell structured nanoparticles," Phys. Rev. B **70**, 235103 (2004).
10. Y. Li, Q. Zhang, A. V. Nurmikko, and S. Sun, "Enhanced magneto-optical response in dumbbell-like Ag–COFe$_2$O$_4$ nanoparticle pairs," Nano Lett. **5**, 1689–1692 (2005).
11. H. Uchida, Y. Masuda, R. Fujikawa, A. V. Baryshev, and M. Inoue, "Large enhancement of Faraday rotation by localized surface plasmon resonance in Au nanoparticles embedded in Bi:YIG film," J. Magn. Magn. Mat. **321**, 843–845 (2009).
12. P. K. Jain, Y. Xiao, R. Walsworth, and A. E. Cohen, "Surface plasmon resonance enhanced magneto-optics (supremo): Faraday rotation enhancement in gold-coated iron oxide nanocrystals," Nano Lett. **9**, 1644–1650 (2009).
13. L. Wang, K. Yang, C. Clavero, A. J. Nelson, K. J. Carroll, E. E. Carpenter, and R. A. Lukaszew, "Localized surface plasmon resonance enhanced magneto-optical activity in core–shell Fe–Ag nanoparticles," J. Appl. Phys. **107**, 09B303 (2010).
14. L. Wang, C. Clavero, Z. Huba, K. J. Carroll, E. E. Carpenter, D. Gu, and R. A. Lukaszew, "Plasmonics and enhanced magneto-optics in core–shell Co–Ag nanoparticles," Nano Lett. **11**, 1237–1240 (2011).
15. Y. H. Lu, M. H. Cho, J. B. Kim, G. J. Lee, Y. P. Lee, and J. Y. Rhee, "Magneto-optical enhancement through gyrotropic gratings," Opt. Express **16**, 5378–5384 (2008).
16. V. I. Belotelov, I. A. Akimov, M. Pohl, V. A. Kotov, A. S. Vengurlekar, A. V. Gopal, D. R. Yakovlev, A. K. Zvezdin, and M. Bayer, "Enhanced magneto-optical effects in magneto-plasmonic crystals," Nat. Nanotechnol. **6**, 370–376 (2011).
17. Y. M. Strelniker and D. J. Bergman, "Optical transmission through metal films with a subwavelength hole array in the presence of a magnetic field," Phys. Rev. B **59**, R12763 (1999).
18. A. B. Khanikaev, A. V. Baryshev, A. A. Fedyanin, A. B. Granovsky, and M. Inoue, "Anomalous Faraday effect of a system with extraordinary optical transmittance," Opt. Express **15**, 6612–6622 (2007).
19. E. T. Papaioannou, V. Kapaklis, E. Melander, B. Hjörvarsson, S. D. Pappas, P. Patoka, M. Giersig, P. Fumagalli, A. Garcia-Martin, and G. Ctistis, "Surface plasmons and magneto-optic activity in hexagonal Ni anti-dot arrays," Opt. Express **19**, 23867–23877 (2011).
20. M. Quinten, A. Leitner, J. R. Krenn, and F. R. Aussenegg, "Electromagnetic energy transport via linear chains of silver nanoparticles," Opt. Lett. **23**, 1331–1333 (1998).
21. M. L. Brongersma, J. W. Hartman, and H. A. Atwater, "Electromagnetic energy transfer and switching in nanoparticle chain arrays below the diffraction limit," Phys. Rev. B **62**, R163356 (2000).
22. S. A. Maier, P. G. Kik, and H. A. Atwater, "Optical pulse propagation in metal nanoparticle chain waveguides," Phys. Rev. B **67**, 205402 (2003).
23. W. H. Weber and G. W. Ford, "Propagation of optical excitations by dipolar interactions in metal nanoparticle chains," Phys. Rev. B **70**, 125429 (2004).
24. D. S. Citrin, "Plasmon polaritons in finite-length metal–nanoparticle chains: the role of chain length unravelled," Nano Lett. **5**, 985–989 (2005).
25. A. L. Fructos, S. Campione, F. Capolino, and F. Mesa, "Characterization of complex plasmonic modes in two-dimensional periodic arrays of metal nanospheres," J. Opt. Soc. Am. B **28**, 1446–1458 (2011).
26. S. Campione, S. Steshenko, M. Albani, and F. Capolino, "Complex modes and effective refractive index in 3D periodic arrays of plasmonic nanospheres," Opt. Express **19**, 26027–26043 (2011).
27. F. Rüting, "Plasmons in disordered nanoparticle chains: localization and transport," Phys. Rev. B **83**, 115447 (2011).
28. Y. Hadad and B. Z. Steinberg, "Magnetized spiral chains of plasmonic ellipsoids for one-way optical waveguides," Phys. Rev. Lett. **105**, 233904 (2010).
29. Y. Mazor and B. Z. Steinberg, "Longitudinal chirality, enhanced nonreciprocity, and nanoscale planar one-way plasmonic guiding," Phys. Rev. B **86**, 045120 (2012).
30. S. Pakdel and M. Miri, "Faraday rotation and circular dichroism spectra of gold and silver nanoparticle aggregates," Phys. Rev. B **86**, 235445 (2012).
31. S. Tomita, T. Kato, S. Tsunashima, S. Iwata, M. Fujii, and S. Hayashi, "Magneto-optical Kerr effects of yttrium-iron garnet thin films incorporating gold nanoparticles," Phys. Rev. Lett. **96**, 167402 (2006).
32. Y. Mizutani, H. Uchida, Y. Masuda, A. V. Baryshev, and M. Inoue, "Magneto-optical plasmonic Bi:YIG composite films with Ag and Au-Ag alloy particles," J. Magn. Soc. Jpn. **33**, 481–484 (2009).
33. A. F. Koenderink, R. de Waele, J. C. Prangsma, and A. Polman, "Experimental evidence for large dynamic effects on the plasmon dispersion of subwavelength metal nanoparticle waveguides," Phys. Rev. B **76**, 201403 (2007).
34. R. Alcazar de la Osa, J. M. Saiz, F. Moreno, and P. Vavassori, "Transverse magneto-optical effects in nanoscale disks," Phys. Rev. B **85**, 064414 (2012).
35. P. B. Johnson and R. W. Christy, "Optical constants of the noble metals," Phys. Rev. B **6**, 4370–4379 (1972).
36. S. Wittekoek, T. J. A. Popma, J. M. Robertson, and P. F. Bongers, "Magneto-optic spectra and the dielectric tensor elements of bismuth-substituted iron garnets at photon energies between 2.2–5.2 eV," Phys. Rev. B **12**, 2777–2788 (1975).
37. X.-X. Liu and A. Alu, "Subwavelength leaky-wave optical nano-antennas: directive radiation from linear arrays of plasmonic nanoparticles," Phys. Rev. B **82**, 144305 (2010).
38. C. Tserkezis and N. Stefanou, "Calculation of waveguide modes in linear chains of metallic nanorods," J. Opt. Soc. Am. B **29**, 827 (2012).
39. D. S. Citrin, "Plasmon-polariton transport in metal-nanoparticle chains embedded in a gain medium," Opt. Lett. **31**, 98–100 (2006).
40. I. B. Udagedara, I. D. Rukhlenko, and M. Premaratne, "Surface plasmon-polariton propagation in piecewise linear chains of composite nanospheres: the role of optical gain and chain layout," Opt. Express **19**, 19973–19986 (2011).

41. P. Holmström, L. Thylen, and A. Bratkovsky, "Composite metal/quantum-dot nanoparticle-array waveguides with compensated loss," Appl. Phys. Lett. **97**, 073110 (2010).
42. D. G. Baranov, A. P. Vinogradov, A. A. Lisyansky, Y. M. Strelniker, and D. J. Bergman, "Magneto-optical spaser," Opt. Lett. **38**, 2002–2004 (2013).
43. M. I. Stockman, "Nanoplasmonics: past, present, and glimpse into future," Opt. Express **19**, 22029–22106 (2011).
44. A. A. Zyablovsky, A. V. Dorofeenko, A. A. Pukhov, and A. P. Vinogradov, "Lasing in a gain slab as a consequence of the causality principle," J. Commun. Techn. Electr. **56**, 1139–1145 (2011).
45. S. Solimeno, B. Crosignani, and P. Di Porto, *Guiding, Diffraction, and Confinement of Optical Radiation* (Academic, 1986).
46. D. G. Baranov, E. S. Andrianov, A. P. Vinogradov, and A. A. Lisyansky, "Exactly solvable toy model for surface plasmon amplification by stimulated emission of radiation," Opt. Express **21**, 10779–10791 (2013).
47. A. L. Rogach, *Semiconductor Nanocrystal Quantum Dots* (Springer, 2008).
48. A. L. Burin, M. A. Ratner, H. Cao, and S. H. Chang, "Random laser in one dimension," Phys. Rev. Lett. **88**, 093904 (2002).
49. S. Wuestner, A. Pusch, K. L. Tsakmakidis, J. M. Hamm, and O. Hess, "Overcoming losses with gain in a negative refractive index metamaterial," Phys. Rev. Lett. **105**, 127401 (2010).
50. http://www.sigmaaldrich.com/materials-science/nanomaterials/lumidots.html.